PCCP

Accepted Manuscript

ROYAL SOCIETY OF CHEMISTRY

www.rsc.org/pccp

Journal Name

ARTICLE

Porphyrin-based graphene oxide frameworks with ultra-large d-spacings for eletrocatalyzation of oxygen reduction reaction

Received 00th January 20xx,
Accepted 00th January 20xx

DOI: 10.1039/x0xx00000x

www.rsc.org/

Bowen Yao,[a] Chun Li,[a] Jun Ma,[b] and Gaoquan Shi[a,*]

Graphene oxide frameworks (GOFs) have attracted a great deal of attention because of their unique functional building blocks, and tunable structures and properties. Herein, a series of porphyrin-based GOFs with crystalline lamellar structures were synthesized via the esterification between boronic acid groups of porphyrins and hydroxyl groups of GO sheets. These GOFs have ultra-large d-spacings up to 26.0 Å, and they were reduced by facile electrochemical reduction. The resulting reduced GOFs (rGOFs) can be used as the catalysts for oxygen reduction reaction (ORR). Electrochemical reduction improved the conductivities of GOFs, accelerating the charge transfer of ORR. The rGOF with Co-porphyrin showed the most positive onset potential of ORR at 0.89 V (vs. RHE, reversible hydrogen electrode), while the rGOF with Fe-porphyrin exhibited the highest catalytic efficiency through an approximately four-electron process. This study provides a new insight for the development of GOFs using multi-functional macrocyclic molecules, revealing their promising applications in electrocatalysts.

Introduction

GOFs are a class of porous materials with crystalline lamellar structures, consisting of graphene oxide (GO) sheets covalently interconnected by rigid molecules.[1–5] GOFs usually have controllable pore sizes and tuneable d-spacings of GO sheets.[6, 7] For instance, Hung et al. reported GOFs with d-spacings varied ranging from 10.4 to 8.7 Å by using diamines of different chain lengths as the crosslinking agents, and they used GOF membranes to separate an ethanol/water mixture through pervaporation.[8] However, up to date, the GOFs with d-spacings larger than 12.0 Å have not yet been reported, while they can provide larger free-volumes for the diffusion of reactant and electrolyte molecules during electrochemical processes.

Porphyrins are macrocyclic molecules with fascinating optical, electronic and catalytic properties; thus they have been widely used as the building blocks to synthesize porous materials such as metal-organic frameworks (MOFs),[9] covalent organic frameworks (COFs)[10] and conjugated meso- and microporous polymers (CMPs).[11] Porphyrins,[12–27] carbon materials[28,29] and their composites[30–39] have also been widely explored to replace precious Pt catalyst for catalysing ORR in fuel cells.[40,41] Their performances depend on their compositions, morphologies and chemical structures.[42–45] On the basis of these considerations, herein, we use 5, 10, 15, 20-tetrakis [4-(dihydroxyboryl) phenyl] porphine (TBPP) and its manganese, iron and cobalt derivatives as molecular pillars of GO sheets to synthesize porphyrin-based GOFs with ultra-large d-spacings up to 26.0 Å (Fig. 1). These GOFs are further electrochemically reduced to form reduced GOFs (rGOFs), and subsequently used as the electrocatalysts for ORR. The reduction increased the electrical conductivity of GO,[38, 46] accelerating the charge transfer of ORR. The Co-porphyrin incorporated rGOF showed the highest electrocatalytic activity with an onset potential of 0.89 V (vs. RHE), while the Fe-porphyrin-based rGOF exhibited the highest catalytic efficiency through a nearly four-electron process.

Experimental Section

Materials

Graphite (1200 mesh) was purchased from Qingdao Huatai Co., Ltd (Qingdao, China). Pinacol [4-(aldehyde) phenyl] boronate was bought from Sukailu Co., Ltd (Suzhou, China). Pyrrole and Nafion solution were obtained from Alfa Aesar Co. The other chemicals were purchased from Beijing Chemical Industry Co., Ltd (Beijing, China). All of them were used directly without purification.

Syntheses

GO and TBPP. GO was synthesized by a modified Hummers method reported by our group, using 1200 mesh graphite particles as the starting material.[47] The GO dispersion was purified by dialysis and freeze-dried before use. TBPP was also synthesized according to literature (Fig. S1, S2, ESI†).[48]

[a] Department of Chemistry, Tsinghua University, Beijing 100084, People's Republic of China. Fax: 86 62771149; Tel: 86 6277 3743. E-mail: gshi@tsinghua.edu.cn.
[b] School of Engineering, University of South Australia, SA 5095, Australia.
†Electronic Supplementary Information (ESI) available: [Supplementary Figures S1-S11 and Table S1].
DOI: 10.1039/x0xx00000x

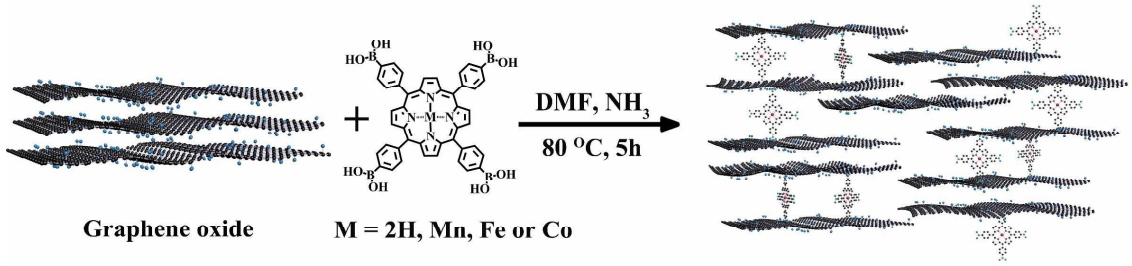

Fig. 1 The procedures for the synthesis of GOFs. Blue balls represent oxygen atoms

Mn-TBPP. TBPP (200 mg, 0.24 mmol) and $MnCl_2 \cdot 4H_2O$ (142 mg, 0.72 mmol) were added to 100 mL anhydrous N,N-dimethylformamide (DMF) in a dried 250 mL flask. The solution was stirred at 100°C for 24 h. After the solution was cooled to room temperature, HCl solution (3 M, 20 mL) was added dropwise. The crude product was precipitated from the solution, and it was collected by filtration, washed with HCl solution (3 M, 20 mL) and water (20 mL) for three times, respectively. A blue solid in 76% yield was obtained. MALDI-TOF-MS: m/z calcd. for $C_{44}H_{32}B_4MnN_4O_8$ 842.93; found 842.95 (Fig. S1, S2, ESI†)

Fe-TBPP. TBPP (200 mg, 0.24 mmol) and $FeCl_2 \cdot 4H_2O$ (300 mg, 2.4 mmol) were added to 100 mL anhydrous DMF in a dried 250 mL flask, and the solution was stirred at 100 °C for 24 h under N_2 atmosphere. Following a procedure the same to that of synthesizing Mn-TBPP, a brownish red solid was obtained in 87% yield. MALDI-TOF-MS: m/z calcd. for $C_{44}H_{32}B_4FeN_4O_8$ 843.84; found 843.95. (Fig. S1, S2, ESI†)

Co-TBPP: TBPP (200 mg, 0.24 mol) and $CoCl_2 \cdot 6H_2O$ (170 mg, 0.72 mmol) were added to 100 mL anhydrous DMF in a dried 250 mL flask. Following a procedure the same to that of synthesizing Mn-TBPP, a purple blue solid was obtained in 82% yield. MALDI-TOF-MS: m/z calcd. for $C_{44}H_{32}B_4CoN_4O_8$ 846.92; found 846.9482. (Fig. S1, S2, ESI†)

P-GOF. Typically, TBPP (15 mg, 19 μmol) and GO (10 mg) were mixed in 10 mL DMF and put into a 20 mL flat bottom flask, and successively the mixture was sonicated for 5 min to form a homogenous dispersion. Then, the dispersion was transferred into a 25 mL pyrex tube (25 mm×100 mm), ammonia solution (25 mg mL^{-1}, 120 μL) was then added to adjust its pH. The viscosity of the solution increased immediately; thus the tube was shaken by vortex vibration and then heated to 80°C for 5 h. During the reaction, the tube was shaken three times. Subsequently the obtained mixture was centrifuged at 10,000 rpm to remove the supernatant, followed by washing with anhydrous acetone and ethanol three times, respectively, to remove the unreacted TBPP. Finally, a light-red powder of P-GOF was obtained after drying at 40°C.

Mn- Fe- and Co-GOFs. GO (10 mg) and Mn-TBPP (16 mg, 19 μmol) or Fe-TBPP (16 mg, 19 μmol), or Co-TBPP (16 mg, 19 μmol) were added into 10 ml DMF in a 20 mL flat bottom flask. Then, the dispersion was transferred into a 25 mL pyrex tube (25 mm×100 mm), ammonia solution (25 mg mL^{-1}, 120 μL) was then added to adjust its pH value. The following procedures were the same with those used for the synthesis of P-GOF.

GO control. GO (10 mg) was added into 10 mL DMF in a 20 mL flat bottom flask without adding ammonia. Successively, it was heated at 80°C for 5 h. The following purification procedures were the same with those used for the synthesis of P-GOF.

Ammonia treated GO (GO_{NH3}). GO (10 mg) and ammonia solution (25 mg mL^{-1}, 120 μL) was added into 10 ml DMF in a 20 mL flat bottom flask. Successively, it was heated at 80°C for 5 h. The following purification procedures were the same with those used for the synthesis of P-GOF.

GO/Co-TBPP mixture. GO (10 mg) and Co-TBPP (10 mg) were added into 10 ml DMF in a 20 mL flat bottom flask without adding ammonia. The following procedures were the same with those used for the synthesis of P-GOF.

Characterizations

X-ray diffraction (XRD) examinations were carried out on a Rigaku D/max-2500/PC X-ray diffractometer equipped with a Cu Kα ray (λ=1.54184 Å) as the incident beam. Nitrogen sorption isotherms were taken out at 77 K using a quantachrome SI–MP analyser, prior to measurements, the samples were degassed in vacuum at 80°C for 6 h. Specific surface areas were measured by a Brunauer-Emmett-Teller (BET) method. Thermal gravimetric analysis (TGA) was conducted on a METTLER TOLEDO instrument. Raman spectra were obtained on a Renishaw Raman microscope with a 514-nm laser. Fourier transform infrared (FT-IR) spectra were recorded on a Bruker Vertex V70 infrared spectrometer. Matrix-assisted laser desorption ionization time-of-flight mass (MALDI-TOF MS) spectra were taken out using an ABI 5800 instrument. Scanning electron micrographs (SEM) were collected on a field-emission scanning electron microscope (Sirion-200, Japan). For SEM studies, GOFs and GO powers were dispersed in ethanol with a weak sonication, and then the supernatants were drop dried on silicon wafers.

Electrochemical measurements

4 mg of catalyst and 50 μL of Nafion solution (5%, by weight) was added into the 950 μL ethanol and then sonicated for 1 h to form a homogeneous dispersion. 12.5 μL of the dispersion was drop casted

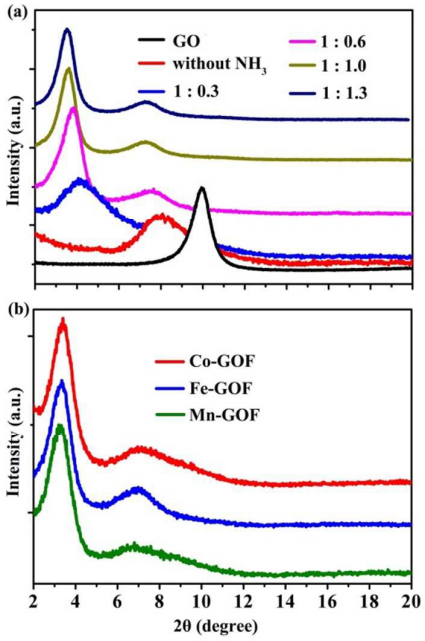

Fig. 2 (a) XRD of GO control, the products synthesized without ammonia, and the GOFs with different mass ratios of GO to TBPP. (b) XRD of Co-GOF, Fe-GOF and Mn-GOF.

to the surface of glassy carbon electrode (GCE, area = 0.25 cm^2), giving a mass loading of catalyst of 0.2 mg cm^{-2}.

Electrochemical measurements were carried out in a three-electrode system by the use of an electrochemical workstation (CHI 760D, CH instrument, Inc.). rGOF modified GCE was used as the working electrode and a platinum net was used as the counter electrode. The potentials were referred to a KCl saturated silver/silver chloride (Ag/AgCl) electrode. The electrolyte was an aqueous solution of 0.1 M KOH. Cyclic voltammetric (CV) study was carried out in the potential range of 1.2 to 0.2 V. Prior to each measurement, the electrolyte was bubbled with either N_2 or O_2 for 30 min to ensure that the solution either deaerated or saturated with O_2; the electrode was then treated by CV scanning for 10 cycles at 50 mV s^{-1} to achieve a stable cycle.

Rotating disk electrode (RDE) measurements were performed by using a MSRX electrode rotator (Pine Instrument) in the potential range of 1.2 to 0.2 V at a scan rate of 50 mV s^{-1} with rotating speeds ranging from 400 to 2025 rpm.

Rotating ring-disk electrode (RRDE) measurements were performed on a MSRX electrode rotator in the potential range of 0.2 to –0.8 V at a scan rate of 50 mV s^{-1} with a rotating speed of 1600 rpm. The ring potential was fixed at 0.5 V.

Two methods can be used to calculate the electron transfer number of ORR at the working electrode.[49] The first one is based on the Koutecky–Levich equation:

$$\frac{1}{J} = \frac{1}{J_L} + \frac{1}{J_K} = \frac{1}{B\omega^{1/2}} + \frac{1}{J_K}$$

$$B = 0.2nFC_o\,(D_o)^{2/3}\nu^{-1/6}$$

where J is the measured current density, J_K and J_L are the kinetic- and diffusion-limiting current densities, ω is the angular velocity, n is transferred electron number, F is the Faraday constant (96 485 C mol^{-1}), C_o is the concentration of O_2 (1.2×10^{-6} mol cm^{-3}), D_o is the diffusion coefficient of O_2 (1.9×10^{-5} cm^2 s^{-1}), and ν is the kinematic viscosity of the electrolyte (0.01 cm^2 s^{-1}). The constant 0.2 is adopted when the rotation speed is expressed in rpm. n can be derived from the slope of the K-L plot (1/J vs. $\omega^{-1/2}$) based on RDE measurements.

The second one is based on RRDE measurements, using the following equations:

$$n = 4 \times \frac{I_d}{I_d + I_r/N}$$

$$\%\,HO_2^- = 200 \times \frac{I_r/N}{I_d + I_r/N}$$

where I_d is the faradic disk current, I_r is the faradic ring current, and N is the collection efficiency of ring electrode, calculated to be 0.33 when the disk electrode was modified with Co-rGOF (Fig. S3, ESI†).

All the potentials were reported versus RHE except those specially mentioned.

Result and Discussion

TBPP and its Mn, Fe, and Co derivatives were used as the building blocks to react with the hydroxyl groups of GO sheets to form GOFs (Fig. 1), and the products are denoted by P-GOF, Mn-GOF, Fe-GOF and Co-GOF, respectively. The structures of GO and GOFs were characterized by X-ray diffraction (XRD) (Fig. 2a). The XRD pattern of GO shows a (001) diffraction peak centred at

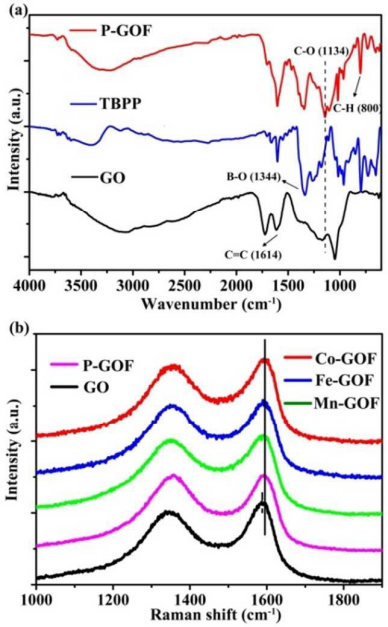

Fig. 3 (a) IR spectra of GO, TBPP and P-GOFs. (b) Raman spectra of GO and GOFs

2θ = 10.0° with a d-spacing of 8.9 Å; this value is close to that of the GO reported in literature.[50] As a certain amount of TBPP (1:1, weight ratio of TBPP to GO) was blended into GO, an amorphous solid product was obtained. Its XRD pattern shows a wide diffraction peak at around 2θ = 8.0° with a d-spacing of 11.0 Å. This value is much smaller than the length of a TBPP molecule, possibly due to that the TBPP molecules are laying on the surfaces of GO sheets through π-π interaction. In this case, the strong acidity of the carboxyl groups of GO prevented the condensation reaction between TBPP and GO. Therefore, a little amount of ammonia solution (25 mg mL^{-1}, 120 μL) was added to the reaction system to neutralize the acidity of GO. The solid obtained from this system showed a broad diffraction at around 2θ = 4.21° with a d-spacing of 21.1 Å, indicating the successful esterification between TBPP and GO to form a GOF with low crystallinity. Upon increasing the TBPP/GO mass ratio from 0.3:1 to1.3:1, the XRD peaks of GOFs shifted to smaller angles from 2θ = 4.21° to 3.53° with narrower peak widths, corresponding to the d-spacings from 21.1 Å to 24.8 Å. The residual weak diffraction at around 2θ = 7.50° is assigned to the GO sheets coated with laid TBPP molecules. Manganese, iron and cobalt porphyrins were used to synthesize of corresponding Mn-GOF, Fe-GOF, Co-GOF, and their XRD patterns demonstrate characteristic diffractions at 2θ = 3.30° (26.8 Å), 3.34° (26.4 Å) and 3.40° (26.0 Å), respectively (Fig. 2b). The large d-spacings indicate the successful formation of GOFs; the rigid porphyrin molecules expanded the interlayer distances of GO sheets. The morphologies of these GOFs are similar to that of GO, having layered microstructures (Fig. S4, S5, ESI†). The GOFs are not perfect crystals, while they show some crystalline features. The GO sheets are flexible, their lateral dimensions are not uniform and their oxidized domains are disordered clusters. It is noteworthy that amorphous phases are also unavoidably presented in other frameworks such as MOFs, COFs and phenylenebisboronic acid based GOFs.[1,9] On the other hand, the porphyrin based GOFs still have incompletely reacted TBPP and GO after purification. The scheme shown in Fig. 1 has demonstrated these situations. The incomplete expansion of GO sheets and the formation of frameworks are facilitate to improve the conductivities of GOFs after reduction.

Infrared and Raman spectral studies also confirmed the successful incorporation of TBPP, Mn-, Fe-, or Co-porphyrin into GO. The IR spectrum of GO shows the following characteristic peaks: C=O (1725 cm^{-1}), C=C (1614 cm^{-1}), C–O(1200 cm^{-1}), C–O–C (1041 cm^{-1}) and O–H (3200 cm^{-1}) (Fig. 3a).[47] The characteristic IR peaks of TBPP are listed as follows: O–H (3400 cm^{-1}), C=C (1605 cm^{-1}), B–O (1346 cm^{-1}), B–C (1255 and 1016 cm^{-1}), N–H (966 cm^{-1}), C–H (800, 723 and 650 cm^{-1}).[48] In the spectrum of P-GOF, the 1608, 1344, and 1022 cm^{-1} are assigned to C=C, B–O, and B–C bonds. The new peak at 1143 cm^{-1} reflects the formation of boronic ester bonds, indicating the successful incorporation of TBPP into GO to form P-GOF. The IR spectra of Mn-, Fe-, Co-GOFs are similar to that of P-GOF (Fig. S6, ESI†). Raman spectra of GO have two characteristic bands at 1588 and 1344 cm^{-1}, corresponding to the G- and D- bands of carbon materials (Fig. 3b). The G-band is associated with in-plane vibration of sp^2 C=C bonds. When the electron density of GO was

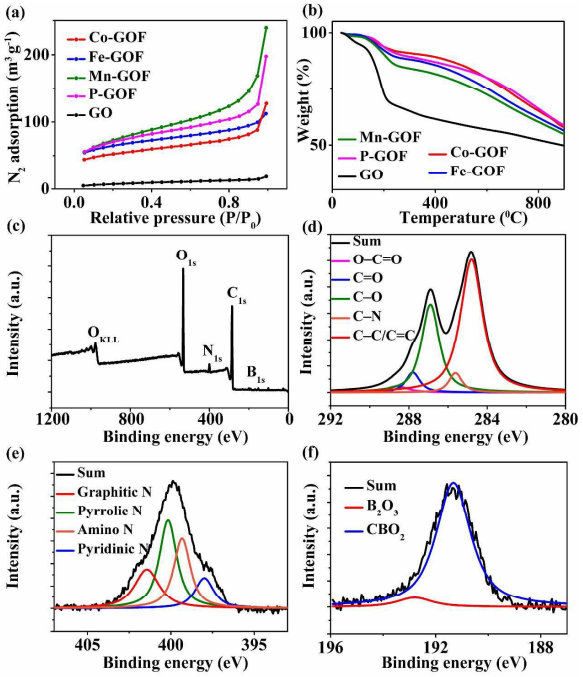

Fig. 4 Nitrogen adsorption isotherms (a) and TGA (b) of GOFs and GO. XPS survey scan spectra (c), C1s spectra (d), N1s spectra (e) and B1s (f) spectra of P-GOF.

changed, the position of its G- band usually showed a blue- or red-shift, indicating the electron transfers from or to GO.[51] TBPP is an electron-deficient molecule because of its boronic acid groups, making electrons transfer from GO sheets to porphyrin. Thus, the G-band of GO in P-GOF was blue-shifted from 1588 cm^{-1} for pure GO to 1592 cm^{-1}. This phenomenon is in consistent with that observed from the esterification between 1,4-diboronic acid and GO.[3] On the other hand, D-band is related to the structural defective domains in graphene sheets, and the D/G band intensity ratio (I_D/I_G) can be used to evaluate the average sizes of the graphitic domains.[47, 52] The I_D/I_G ratios of GOFs are nearly identical to that of GO, reflecting that the graphitic domains of GO were unchanged after the reaction with porphyrins.

The porosities and specific surface areas of GOFs were measured by Brunauer-Emmett-Teller (BET) method under nitrogen atmosphere at 77 K (Fig. 4a). Prior to measurements, the samples were degassed under vacuum at 80°C for 6 h to remove the solvent and water entrapped in the samples. The specific surface areas of GO, P-GOF, Mn-GOF, Fe-GOF, Co-GOF were measured to be 26, 243, 259, 219 and 189 m^2 g^{-1}, respectively. (Fig. S7, ESI†). Meanwhile, the nitrogen adsorption-desorption isotherms of GOFs are Type IV in shapes, indicating they have micro- and meso-porous networks. These BET specific surface areas are comparable to those of the counterparts reported in reference 1, while still not large enough as expected. This phenomenon can be explained as follows. (1) The specific surface areas of GOFs strongly depend on their contents of porphyrin

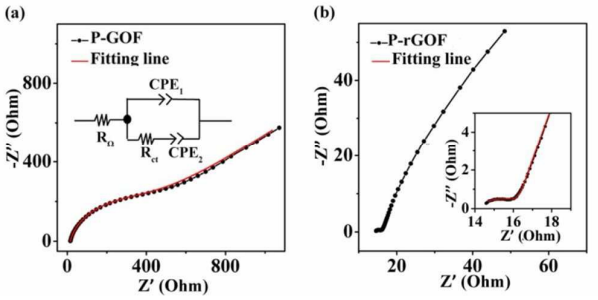

Fig. 5 Nyquist plots of P-GOF (a) and P-rGOF (b) from 10^5 Hz to 1 Hz at an open circuit potential. The EIS of P-GOF from 10^5 to 1 Hz and and EIS of P-rGOF from 10^5 to 10 Hz were fitted by the modified Randles equivalent circuit (inset), where R_Ω represents the electrolyte resistance, R_{ct} represents the charge transfer resistance, and CPE_1 and CPE_2 denote respectively the double layer capacitance and the Warburg-type diffusion resistance (the red line are fitting results).

pillars.[1] When the pillar content was high, the microstructure of GOF was relatively compact with a small amount of accessible pores. If the content of porphyrin pillar was low, GO sheets could not be efficiently expanded. Therefore, the mass ratios of GO and porphyrins have to be optimized to achieve GOFs with acceptable specific surface areas as described above. (2) In GOFs, the incompletely reacted GO sheets were unavoidably stacked with each other through π-π interaction upon drying. This assumption has been confirmed by the residual broad peaks at around $2\theta = 8.0^o$ in the XRD patterns of GOFs (Fig. 2).

The thermal stabilities of GO and GOFs were studied using thermal gravimetric analysis (TGA) (Fig. 4b). The initial weight loss before 100 °C is resulted from the release of the water molecules interacted with GO sheets. The distinct 25% weight loss between 100 and 220 °C is attributed to the unstable oxygen-containing functional groups of GO, and the gradual weight loss at temperatures higher than 250°C is associated with the removal of more stable functional groups. The less weight losses of GOFs before 100 °C reflect their lower water contents, mainly due to the hydrophobic groups grafted to GO. The GOFs also show much lower weight losses than that of GO in the temperature range between 125 and 220°C, reflecting that they have fewer unstable oxygen-containing functional groups because of their esterification with TBPP or its derivatives. The weight loss (20%) at 500 °C relates to the decomposition of porphyrin moieties of GOF. These TGA results also confirm the successful formation of GOFs.

X-ray photoelectron spectroscopy (XPS) was used to analyse the atomic composition and bonding configuration of P-GOF. Table S1 (ESI†) lists the atomic compositions of P-GOF, GO and GO_{NH3} (GO was treated with ammonia at 80°C for 5 h). Accordingly, GO mainly consists of C, O elements and a trace amount of N atoms, while GO_{NH3} has a lower content of oxygen and a higher content of nitrogen (Fig. S8a, S8c, ESI†). This is mainly due to the partial reduction and nitrogen doping of GO by ammonia. P-GOF has C, O, N and B atoms because of the incorporation of TBPP. The C1s and N1s XPS spectra of P-GOF (Fig. 4d-e) are similar to those of GO_{NH3} (Fig. S8d-S8e, ESI†). The C1s spectrum of P-GOF can be divided into five peaks, corresponding to O–C=O (288.6 eV), C=O (287.8 eV), C–O (286.9 eV), C–N (285.6 eV) and C–C/C=C (284.8 eV).[53–55] The N 1s spectrum indicates the presence of four types of N atoms: graphitic N (401.4 eV), pyrrolic N (400.1 eV), Amino N (399.3 eV) and pyridinic N (397.99 eV).[53–55] The B 1s spectrum can be divided into two peaks: oxidized boron states of CBO_2 and B_2O_3, respectively (Fig. 4f, Fig. S8f, ESI†), in consistent with those reported in literature.[3]

It is believed that the electrochemical reduction of oxygen gas is confined at the electrolyte-electrode interface; an ideal interface for ORR should have both high electronic and ionic conductivities.[42] Therefore, the interfacial boundary of electrocatalyst and electrolyte plays a critical role in controlling the performances of the catalysts for ORR. Our GOFs have large d-spacings up to 26 Å, making their surfaces fancily accessible to oxygen molecules. Thus they are expected to be promising cost-effective electrocatalysts for ORR.

Under an ideal condition, the maximum electrical energy applied to perform an electrochemical reaction should equal to the total loss of Gibbs free energy of this reaction. However, a deviation from a thermodynamic equilibrium usually occurs in real reaction, possibly due to activation polarization, mass diffusion, Ohmic resistance, etc.[56] Among these, the electric conductivity of catalysts is an important factor of determining the electrochemical process. Many reducing agents such as hydriodic acid,[57] sodium borohydride[58] and hydrazine[59] can be used to remove the oxygen-containing groups of GO sheets to enhance their conductivity. Considering the sensitivity of boron ester bonds to acidic compounds, and the coordination between hydrazine and transition-metal porphyrins, here we chose electrochemical method for reduction.[46] The GOFs were reduced by cyclic voltammograms (CVs) for 20 cycles in the potential range of 0.96 to –0.44 V at a scan rate of 50 mV s^{-1} in 0.1 M PBS to form reduced GOFs (rGOFs). The resulting rGOFs with different porphyrin building blocks are denoted by P-rGOF, Mn-rGOF, Fe-rGOF, and Co-rGOF, respectively. Electrochemical impedance spectroscopy was used to study the P-GOF or P-rGOF modified electrode in 0.1 mol L^{-1} KCl solution containing 10 mmol L^{-1} $K_3Fe(CN)_6/K_2Fe(CN)_6$. The experimental data were fitted by Randles equivalent circuit, and the fitting lines are consistent with the experimental data (Fig. 5, Fig. S9-11, ESI†).). Through the electrochemical reduction, the charge transfer resistance of P-GOF modified electrode reduced from 305.9 to 2.51 Ω, and the double-layer capacitance increased remarkably from 9.41 μF to 2.04 mF. The electrodes based on Metal-incorporated GOFs also showed similar phenomena (Table S2, ESI†). These results reflect that electrochemical reduction greatly increased the conductivities of GOF modified electrodes, accelerating charge transfer and in favour of forming electrical double-layers.[60]

The catalytic activities of rGOFs were tested by CVs performed in 0.1 M KOH aqueous solution saturated with oxygen or nitrogen in the potential range of 1.15 to 0.165 V (vs. RHE) at a scan rate of 50 mV s^{-1} (Fig. 6a). The CV of P-GOF shows an ORR wave with a peak at 0.25 V and a peak current of 0.15 mA. In comparison with P-rGOF, metal-rGOFs show much enhanced electrocatalytic ORR activities. Among them, the CV of Co-rGOF has the most positive cathodic peak potential at 0.793V, far more positive than 0.664 V for Mn-rGOF and 0.703 V for Fe-rGOF;

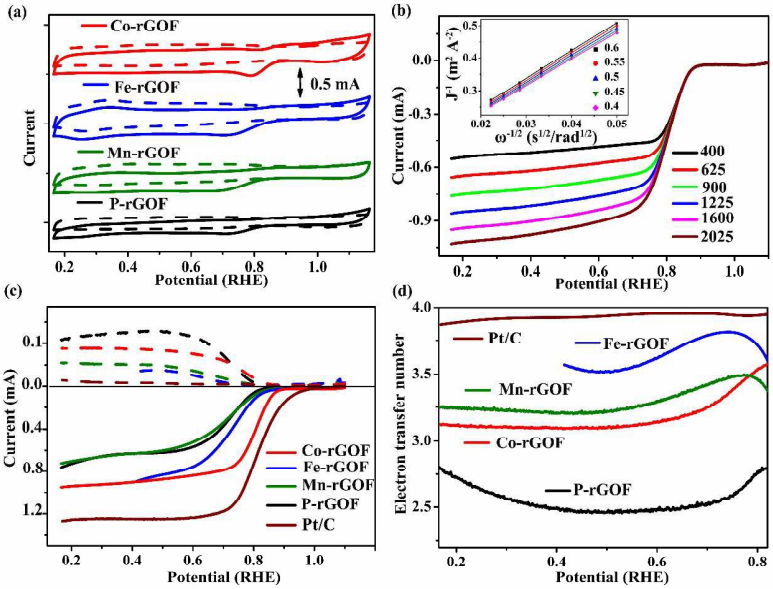

Fig. 6 (a) CVs of ORR on the GOFs modified glassy carbon electrodes in 0.1 M oxygen- or nitrogen-saturated KOH solution at scan rate of 50 mv s^{-1}. (b) RDE measurements of ORR on the Co-GOF modified glassy carbon electrode in 0.1 M oxygen-saturated solution with the rotating speed from 400 to 2025 rpm at the scan rate of 10 mv s^{-1}. (c) RRDE measurements of ORR on the Co-rGOF, Pt/C modified glassy carbon electrode in the 0.1 M oxygen-saturated solution with the rotating speed of 1600 rpm at the at the scan rate of 10 mv s^{-1}, ring electrode was fixed at 0.5 V. (d) Comparison of electron transfer number of ORR on the different GOFs modified electrodes using RRDE measurements

the CV of Fe-rGOF also has a pair of weak redox waves at 0.25 V/0.33 V with onset potentials of 0.36 V/0.21 V. These waves are assigned to the redox of Fe-porphyrin. In order to investigate relevant electrocatalytic mechanism, linear sweep voltammetric (LSV) measurements were carried out under different rotating rates in oxygen-saturated 0.1 M KOH solution at a scan rate of 10 mV s^{-1} (Fig. 6b). Each LSV curve of rGOFs shows a stable current at low potentials, indicating a sufficiently rapid charge-transfer at the electrolyte-electrode interface; the reaction rate was controlled by concentration polarization (Fig. S12a-f, ESI†). The LSV curve of P-rGOF electrode shows an onset potential at 0.82 V, and its limit current density and kinetic limiting current are 0.60–0.75 mA and 2.15–2.58 mA. For comparison, all of the metal-rGOFs exhibited electrocatalytic activities stronger than that of P-rGOF. The LSV curve of Co-rGOF has the most positive onset potential of 0.89 V and the strongest kinetic limiting current density of 3.35 mA at 0.5 V reflecting its smallest activation polarization and fastest electrochemical reaction. The metallic porphyrin can form a transition complex with oxygen molecule, decreasing the bonding energy of oxygen to facilitate its reduction. Therefore, the metal porphyrin processes higher activity. Moreover, compared with the Fe- or Mn-GOF, the better performance of the Co-GOF is related to the unique electron configuration of the d orbitals of Co-porphyrin (empty d_{x^2} orbitals and filled d_{xz} and d_{yz} orbitals probably are two requirements) according to the molecular orbital theory. [12] The CV of Fe-rGOF has a pair of weak redox waves at 0.25 V/0.33 V (Fig. 6a). Thus, the currents of LSV recorded at the potentials lower than 0.45 V cannot reflect its ORR activity, thus not shown in Fig. 6c.

ORR usually undergoes two different processes:[61] direct four-electron pathway ($O_2 + 2H_2O + 4e^- \rightarrow 4OH^-$, $\varphi^{\ominus}$=0.40 V (vs. SHE, standard hydrogen electrode) and indirect two-electron pathway ($O_2 + H_2O + 2e^- \rightarrow HO_2^- + OH^-$, $\varphi^{\ominus}$= −0.08 V (vs. SHE) and $HO_2^- + H_2O + 2e^- \rightarrow 3OH^-$, $\varphi^{\ominus}$=0.88 V (vs. SHE). The latter process reduces the voltages of fuel cells, and its intermediate peroxide has a negative effect on electrode materials.[30] In order to verify the ORR efficiency on the rGOF modified electrodes, the transferred electron number per oxygen molecule (n) in ORR can be used as an evaluation parameter, and it can be calculated by the Koutecky−Levich (K−L) equation. The K-L plots of all rGOF electrodes have a good linearity (Fig. 6b). The values of n measured at different potentials are shown in Fig. S13 (ESI†). Accordingly, the n for ORR at Fe-rGOF electrode was estimated to be 3.9–4.0, higher than those at the Co-rGOF (3.2–3.5), Mn-rGOF (3.4–3.5) and P-rGOF (2.3–2.5) electrodes. These results indicate that the ORR at the Fe-rGOF electrode works mainly through a four-electron process, while that at P-rGOF is predominately a two-electron process. The ORR pathway was also studied by monitoring the intermediate peroxide species of HO_2^- through using a disk Rotation ring disk electrode (RRDE). The electron transfer numbers calculated from RRDE measurements are consistent with those derived from K-L plots (Fig. 6c-d). Fe-rGOF catalysed the ORR through mainly four-electron process with n= 3.5-3.8, while the ORR at P-rGOF electrode followed a *quasi* two-electron process with n= 2.4–2.7. Accordingly, Fe-rGOF can catalyse ORR with the smallest peroxide yield of 9−24% while the P-rGOF has the highest yield of 60−78% (Fig. S14, ESI†). However, in RRDE analysis, the released H_2O_2 might be reduced by neighbouring catalyst molecules before being detected by the ring electrode, because Fe-porphyin also can catalyse the reduction

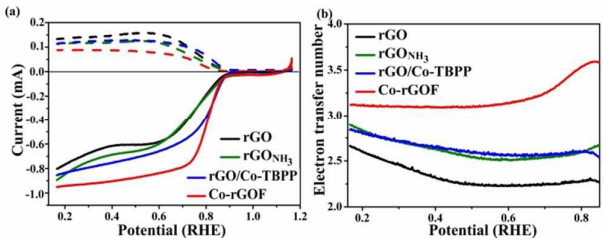

Fig. 7 (a) RRDE curve of ORR at rGO, rGO_{NH3}, rGO/Co-TBPP mixture or Co-rGOF modified electrode. (b) Electron transfer number of ORR at different electrodes.

of H_2O_2.[62] Thus, the kinetic process of Fe-rGOF catalyzation is still unclear, requiring further investigation.[63]

rGO and rGO_{NH3} electrodes were prepared by the electrochemical reduction of GO control and GO_{NH3}. The catalytic activities of rGO, rGO_{NH3} and P-rGOF were compared by RRDE examinations (Fig. 7). The RRDE curve of GO electrode shows the lowest current (–0.8 mA) and the lowest electron transfer number (2.2–2.6). The electron transfer number and current of rGO_{NH3} electrode are slightly higher than those of GO electrode because of the nitrogen doping effect. The ORR performance of P-rGOF electrode is comparable to that of GO_{NH3}, indicating that the boron atoms did not improve its catalytic activity. Moreover, we also prepared a rGO/Co-TBPP mixture without adding ammonia, and it showed a weaker current (–0.85 mA) and a smaller electron transfer number (2.8–2.6) than those of Co-rGOF. This is mainly due to that Co-rGOF has an expanded framework with a large d-spacing, providing more accessible catalytic site.

Commercial Pt/C showed a better catalytic performance than those of GOFs (Fig. 6c, Fig. S12g, Fig. S10h, ESI†); however, it usually suffers from its low electrochemical stability and methanol-crossover effect (Fig. 8).[64] In order to study the durability and methanol crossover of rGOF electrodes, chronoamperometric measurements were carried out in 0.1 M KOH at 0.5 V with constant oxygen flow. All of the rGOF electrodes showed similar long-term electrochemical stability with a retention of about 87% after a 12,000 s test at 0.5 V and almost free from the methanol crossover effect. In contrast, the Pt/C electrode exhibited a retention of only 72% and a severe methanol crossover effect under the same test condition.

Conclusions

Porphyrin-based GOFs with crystalline lamellar structures have been successfully synthesized through boronate condensation. They have large d-spacings and thus much higher specific surface areas than that of their GO precursor. rGOFs have strong catalytic activities for ORR and their performances depend on their metal ions. Co-rGOF showed the strongest catalytic activity, while the Fe-rGOF can catalyse ORR by a *quasi* 4-electron mechanism. The porous microstructures and the porphyrin building blocks are tuneable for modulating the catalytic performances of GOFs. The rGO component provides the catalysts with high electrical conductivity for charge transfer. This work is the first example of constructing GOFs with large d-spacings and promising electrocatalytic performances by using functional porphyrin molecules and GO sheets as building blocks.

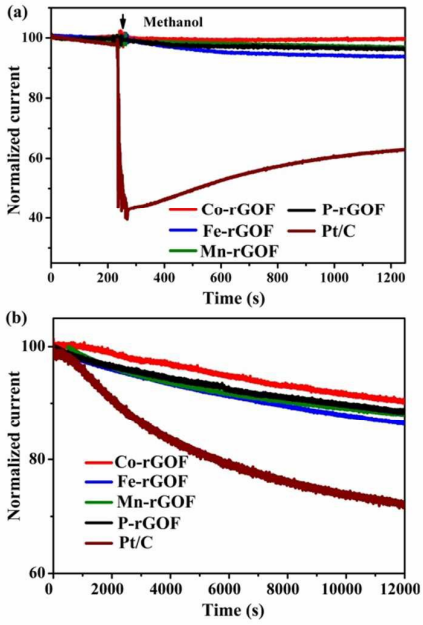

Fig. 8 Methanol crossover (a) and durability (b) of rGOF and Pt/C modified electrodes. Chronoamperometric measurements were conducted in the oxygen-saturated 0.1 M KOH solution at a rotating speed of 900 rpm, 3 M methanol was added during the measurement.

Acknowledgements

This work was supported by the National Basic Research Program of China (973 Program, 2012CB933402, 2013CB933001), Natural Science Foundation of China (51433005),

Notes and references

1 J. W. Burress, S. Gadipelli, J. Ford, J. M. Simmons, W. Zhou and T. Yildirim, *Angew. Chem. Int. Ed.*, 2010, **49**, 8902–8904.
2 G. Srinivas, J. W. Burress, J. Ford and T. Yildirim, *J. Mater. Chem.*, 2011, **21**, 11323–11329.
3 E. Pourazadi, E. Haque, W. Zhang, A. T. Harris and A. I. Minett, *Chem. Commun.*, 2013, **49**, 11068–11070.
4 R. Kumar, V. M. Suresh, T. K. Maji and C. N. R. Rao, *Chem. Commun.*, 2014, **50**, 2015–2017.
5 G. Srinivas, J. Burress and T. Yildirim, *Energy Environ. Sci.*, 2012, **5**, 6453–6459.
6 A. Nicolai, B. G. Sumpter and V. Meunier, *Phys. Chem. Chem. Phys.*, 2014, **16**, 8646–8654.
7 K. Tae Kyung, C. Jae Yeong, Y. Kyung, K. Jung Woo, H. Sung-min, S. Hyeon Suk, J. Sang Hoof and M. Hoi Ri, *J. Mater. Chem. A.*, 2013, **1**, 8432–8437.
8 W. S. Hung, C. H. Tsou, M. De Guzman, Q. F. An, Y. L. Liu, Y. M. Zhang, C. C. Hu, K. R. Lee and J. Y. Lai, *Chem. Mater.*, 2014, **26**, 2983–2990.
9 D. Feng, Z. Y. Gu, J. R. Li, H. L. Jiang, Z. Wei and H. C. Zhou, *Angew. Chem. Int. Ed.*, 2012, **51**, 10307–10310.

10 X. Feng, L. Liu, Y. Honsho, A. Saeki, S. Seki, S. Irle, Y. Dong, A. Nagai and D. Jiang, *Angew. Chem. Int. Ed.*, 2012, **51**, 2618–2622.
11 Z. H. Xiang, Y. H. Xue, D. P. Cao, L. Huang, J.-F. Chen and L. M. Dai, *Angew. Chem. Int. Ed.*, 2014, **126**, 2465–2469.
12 H. Jahnke, M. Schönborn and G. Zimmermann, in *Physical and Chemical Applications of Dyestuffs*, eds. F. P. Schäfer, H. Gerischer, F. Willig, H. Meier, H. Jahnke, M. Schönborn and G. Zimmermann, Springer Berlin Heidelberg, 1976, vol. 61, ch. 4, pp. 133–181.
13 H. Alt, H. Binder and G. Sandtede, *J. Catal.*, 1973, **28**, 8–19.
14 J. P. Collman, M. Marrocco, P. Denisevich, C. Koval and F. C. Anson, *J. Electroanal. Chem*, 1979, **101**, 117–122.
15 T. Kuwana, *J. Electroanal. Chem*, 1978, **88**, 299–303.
16 A. Bettelheim and T. Kuwana, *Anal. Chem.*, 1979, **51**, 2257–2260.
17 A. Bettelheim, D. Ozer and R. Parash, *J. Chem. Soc., Faraday Trans. 1*, 1983, **79**, 1555–1564.
18 A. Bettelheim, R. Parash and D. Ozer, *J. Electroanal. Soc.*, 1982, **129**, 2247-2250.
19 A. Bettelheim, B. A. White, S. A. Raybuck and R. W. Murray, *Inorg. Chem.*, 1987, **26**, 1009–1017.
20 D. A. Buttry and F. C. Anson, *J. Am. Chem. Soc.*, 1984, **106**, 59–64.
21 J. P. Collman, P. Denisevich, Y. Konai, M. Marrocco, C. Koval and F. C. Anson, *J. Am. Chem. Soc.*, 1980, **102**, 6027-6036.
22 R. R. Durand, C. S. Bencosme, J. P. Collman and F. C. Anson, *J. Am. Chem. Soc.*, 1983, **105**, 2710–2718.
23 S. Fukuzumi, S. Mochizuki and T. Tanaka, *Inorg. Chem.*, 1990, **29**, 653–659.
24 N. Kobayashi and W. A. Nevin, *Appl. Organomet. Chem.*, 1996, **10**, 579–-590.
25 D. Ozer, R. Parash, F. Broitman, U. Mor and A. Bettelheim, *J. Chem. Soc., Faraday Trans. 1*, 1984, **80**, 1139–1149.
26 K. Shigehara and F. C. Anson, *J. Phys. Chem.*, 1982, **86**, 2776–2783.
27 B. D. Matson, C. T. Carver, A. Von Ruden, J. Y. Yang, S. Raugei and J. M. Mayer, *Chem. Commun.*, 2012, **48**, 11100–11102.
28 J. Liang, Y. Jiao, M. Jaroniec and S. Z. Qiao, *Angew. Chem. Int. Ed.*, 2012, **51**, 11496–11500.
29 Y. Liang, Y. Li, H. Wang, J. Zhou, J. Wang, T. Regier and H. Dai, *Nat. Mater.*, 2011, **10**, 780–786.
30 I. Kruusenberg, L. Matisen and K. Tammeveski, *J. Nanosci Nanotech.*, 2013, **13**, 621–627.
31 I. Kruusenberg, J. Mondal, L. Matisen, V. Sammelselg and K. Tammeveski, *Electrochem. Commun.*, 2013, **33**, 18–22.
32 G. Faubert, G. Lalande, R. Cote, D. Guay, J. P. Dodelet, L. T. Weng, P. Bertrand and G. Denes, *Electrochim. Acta*, 1996, **41**, 1689–1701.
33 S. L. Gojkovic, S. Gupta and R. F. Savinell, *J. Electroanal. Soc.*, 1998, **145**, 3493–3499.
34 H. Schulenburg, S. Stankov, V. Schunemann, J. Radnik, I. Dorbandt, S. Fiechter, P. Bogdanoff and H. Tributsch, *J. Phys. Chem. B*, 2003, **107**, 9034–9041.
35 M. Tsionsky and O. Lev, *J. Electroanal. Soc.*, 1995, **142**, 2132–2138.
36 I. Hijazi, T. Bourgeteau, R. Cornut, A. Morozan, A. Filoramo, J. Leroy, V. Derycke, B. Jousselme and S. Campidelli, *J. Am. Chem. Soc.*, 2014, **136**, 6348–6354.
37 M. Jahan, Q. Bao and K. P. Loh, *J. Am. Chem. Soc.*, 2012, **134**, 6707–6713.
38 J. M. You, H. S. Han, H. K. Lee, S. Cho and S. Jeon, *Int. J. Hydrogen Energy*, 2014, **39**, 4803–4811.
39 H. J. Tang, H. J. Yin, J. Wang, N. L. Yang, D. Wang and Z. Y. Tang, *Angew. Chem. Int. Ed.*, 2013, **52**, 5585–5589.
40 R. Jasinski, *Nature*, 1964, **201**, 1212–1213.
41 H. Jahnke and B. Bunsenges, *Physik. Chem.*, 1968, **72**, 1053.
42 S. B. Adler, *Chem. Rev.*, 2004, **104**, 4791–4843.
43 P. A. Christensen, A. Hamnett and D. Linares Moya, *Phys. Chem. Chem. Phys.*, 2011, **13**, 5206–-5214.
44 H. Kim, K. Lee, S. I. Woo and Y. Jung, *Phys. Chem. Chem. Phys.*, 2011, **13**, 17505–17510.
45 D. J. Wasylenko, C. Rodriguez, M. L. Pegis and J. M. Mayer, *J. Am. Chem. Soc.*, 2014, **136**, 12544–12547.
46 H. L. Guo, X. F. Wang, Q. Y. Qian, F. B. Wang and X. H. Xia, *ACS Nano*, 2009, **3**, 2653–2659.
47 J. Chen, B. W. Yao, C. Li and G. Q. Shi, *Carbon*, 2013, **64**, 225–229.
48 X. Feng, L. Chen, Y. Dong and D. Jiang, *Chem. Commun.*, 2011, **47**, 1979–1981.
49 W. Zhang, Z. Y. Wu, H. L. Jiang and S. H. Yu, *J. Am. Chem. Soc.*, 2014, **136**, 14385–14388.
50. Y. Xu, K. Sheng, C. Li and G. Shi, *ACS Nano*, 2010, **4**, 4324–4330.
51. M. Zhang, W. J. Yuan, B. W. Yao, C. Li and G. Q. Shi, *ACS. Appl. Mater. Interfaces*, 2014, **6**, 3587–3593.
52 Y. X. Xu, K. X. Sheng, C. Li and G. Q. Shi, *J. Mater. Chem.*, 2011, **21**, 7376–7380.
53 J. Baojiang, T. Chungui, W. Lei, S. Li, C. Chen, N. Xiaozhen, Q. Yingjie and F. Honggang, *Appl. Surf. Sci.*, 2012, **258**, 3438–3443.
54 I. T. Kim and M. W. Shin, *Mater. Lett.*, 2013, **108**, 33–36.
55 C. Zhang, R. Hao, H. Liao and Y. Hou, *Nano Energy*, 2013, **2**, 88–97.
56 M. Winter and R. J. Brodd, *Chem. Rev.*, 2004, **104**, 4245-4269.
57 S. Pei, J. Zhao, J. Du, W. Ren and H. M. Cheng, *Carbon*, 2010, **48**, 4466–4474.
58. H. J. Shin, K. K. Kim, A. Benayad, S. M. Yoon, H. K. Park, I. S. Jung, M. H. Jin, H. K. Jeong, J. M. Kim, J.-Y. Choi and Y. H. Lee, *Adv. Funct. Mater.*, 2009, **19**, 1987–1992.
59. D. Li, M. B. Muller, S. Gilje, R. B. Kaner and G. G. Wallace, *Nat. Nanotech.*, 2008, **3**, 101–105.
60. Q. He, T. Mugadza, X. Kang, X. Zhu, S. Chen, J. Kerr and T. Nyokong, *J. Power Sources*, 2012, **216**, 67–75.
61 J. Sun, Y. H. Fang and Z. P. Liu, *Phys. Chem. Chem. Phys.*, 2014, **16**, 13733–13740.
62 J. Chen, L. Zhao, H. Bai and G. Q. Shi, *J. Electroanal. Chem.*, 2011, **657**, 34–38.
63 J. P. Collman, R. Boulatov, C. J. Sunderland and L. Fu, *Chem. Rev.*, 2004, **104**, 561–588.
64 Z. Xiang, Y. Xue, D. P. Cao, L. Huang, J. F. Chen and L. M. Dai, *Angew. Chem. Int. Ed.*, 2014, **53**, 2433–2437.